Journal of Nuclear Medicine, published on September 22, 2016 as doi:10.2967/jnumed.116.180059

Biodistribution and Radiation Dosimetry of C-11 Nicotine from Whole Body PET Imaging in Humans

Pradeep K. Garg[*#†], Stephen J. Lokitz[†], Rachid Nazih[#†], and Sudha Garg[#†]

Department of Radiology, Wake Forest University Health Sciences

Winston Salem, NC 27110

[†]Biomedical Research Foundation, Shreveport, LA

: Author for Correspondence:

Pradeep K. Garg

Center for Molecular Imaging and Therapy

P.O. Box 38020

Shreveport, LA 71103

336-413-1817

pgarg@biomed.org

#† Current Address:

Center for Molecular Imaging and Therapy

Biomedical Research Foundation

P.O. Box 38020

Shreveport, LA 71103

Word Count: 4975

ABSRACT

The main focus of this study was to assess the *in vivo* distribution and radiation absorbed dose of ^{11}C-nicotine derived from the whole body Positron emission tomography (PET) imaging in human. **Methods:** After an initial Computed tomography (CT) attenuation scan, ^{11}C-nicotine was administered via an intravenous injection, and dynamic whole body PET scans were acquired in a 3-D mode on 11 normal healthy (5 male, 6 female) subjects. The first scan was acquired in a dynamic acquisition mode for 90 s with the brain in the field of view, followed by a series of 13 whole body PET scans acquired over a 90 min time period. Regions of interest were drawn over organs visible in the reconstructed PET images. Time activity curves were generated, and the residence times were calculated. The radiation absorbed dose for the whole body was calculated by entering the residence time in OLINDA/EXM 1.0 software, to model the equivalent organ dose and the effective dose for a 70 kg man. **Results:** The mean residence times for the ^{11}C-nicotine in the liver, red marrow, brain, and lungs were 0.048 ± 0.010, 0.031 ± 0.005, 0.021 ± 0.004, and 0.020 ± 0.005 h, respectively. The mean effective dose for ^{11}C-nicotine was 5.44 ± 0.67 μSv/MBq. The organs receiving the highest radiation absorbed dose from the ^{11}C-nicotine injection were the urinary bladder wall (14.68 ± 8.70 μSv/MBq), kidneys (9.56 ± 2.46 μSv/MBq), liver (8.94 ± 1.67 μSv/MBq), and the spleen (9.49 ± 3.89 μSv/MBq). The renal system and hepatobiliary systems were the major clearance and excretion routes for radioactivity. **Conclusions:** The estimated radiation dose burden from ^{11}C-nicotine administration is relatively modest. The low radiation dose for ^{11}C-nicotine would allow for multiple PET examinations on the same research subject.

Key Words: C-11 nicotine, radiation absorbed dose, PET dosimetry, whole body PET imaging

INTRODUCTION

The adult smoking rate in the United States has decreased substantially since the hallmark 1964 US Surgeon General's report. Nonetheless, 40 million Americans still smoke regularly, and approximately 400,000 people die each year due to illnesses directly associated with smoking (*1*). Although the various components of tobacco cause different effects, nicotine has been identified as one of the primary chemicals responsible for tobacco addiction in humans (*2,3*). More recently, there has been a steady rise in the use of newly developed nicotine delivery devices (such as e-cigarettes) to replace cigarettes, and their use has now surpassed any other tobacco product, especially amongst high-school students (*4*). There is growing concern amongst the scientific, medical, and regulatory communities over the deleterious impact of nicotine consumption on human health. Aside from the reinforcing action, nicotine perpetuates the smoking habit in humans through the aversive consequences of nicotine withdrawal, a negative reinforcement phenomenon (*5-7*). Neuronal nicotinic acetylcholine receptors have been identified as one of the primary sites of action in the brain for the elicitation of reinforcing effects, dependency, and withdrawal expressions during cessation of smoking (*8-12*). PET imaging is highly useful for studying the impacts of smoking and the targeting of acetylcholine receptor systems. The involvement of nicotinic receptors in brain cholinergic transmission alludes to the role of nicotine in Alzheimer's disease, where a direct relationship exists between nicotinic receptors, cholinergic transmission, and pathologic symptoms (*13-15*). A PET imaging study in patients with neurodegenerative disease showed a significantly reduced uptake of ^{11}C-nicotine in Alzheimer's disease patients in comparison with healthy controls, especially in the frontal and temporal cortex areas (*16-18*), which was in accordance with a strong correlation between nicotine binding in the parietal cortex and performance in a visuospatial ability test (*16*). ^{11}C-nicotine PET has also been useful for investigating the impact of menthol in cigarettes, which can alter nicotine accumulation in the brain (*19*). Another ^{11}C-nicotine PET study we performed earlier showed a slow accumulation of nicotine

in the brains of dependent smokers, which was partially due to a slower release of accumulated nicotine in the lungs (*20*), establishing a direct relationship between nicotine and its pharmacological impacts on human health. These imaging studies further underscore the importance of ^{11}C-nicotine PET in the study of addiction and other *in vivo* neurological functions. Despite multiple publications on the use of ^{11}C-nicotine in humans, there are no published data on the radiation dosimetry of ^{11}C-nicotine. Therefore, the aim of this study was to obtain estimates of radiation dosimetry of ^{11}C-nicotine in humans. We report on the ^{11}C-nicotine *in vivo* distribution, and estimated the radiation dose in humans using whole body PET scans.

MATERIALS AND METHODS

Subjects

This study was approved by the Radiation Safety Committee and the Institutional Review Board of the Wake Forest University Medical Center. Written informed consent was obtained from each participant prior to the PET studies. In total, 11 (5 males, 6 females) healthy non-smokers (mean age 39.1 ± 9.1) and an average weight of 80.3 ± 26.3 kg were enrolled in this study.

Synthesis of ^{11}C-nicotine radiochemistry

^{11}C-nicotine was produced via the *N*-methylation of (S)-nornicotine using ^{11}C-methyltriflate prepared via a previously reported method with minor modifications (*21*). Briefly, ^{11}C-methyltriflate (FXc-Pro module, GEMS, Waukesha, WI) was bubbled through a solution of 0.25 mg (S)-nor-nicotine biscamsylate and 10 μL of 1,2,2,6,6 pentamethyl piperidine in 300 μL of acetonitrile. After the ^{11}C-methyltriflate delivery was complete, the reaction mixture was loaded on the high performance liquid chromatography loop and the desired product was isolated using a semi-preparatory high performance liquid chromatography column (Waters, μPorasil silica 7.8 × 300 mm, 10 μm) eluted with a 96% dichloromethane and 4% methanol/trimethylamine (100/1, v/v), at a flow rate of 2 mL/min.

PET imaging

The PET/CT images were acquired on a GE Discovery VCT PET/CT scanner (GEMS, Waukesha, WI, USA). The imaging characteristics of this scanner have been described previously (*22*). Iterative image reconstruction with measured attenuation correction, modeled scatter correction, and random correction using singles count rates was performed for all subjects (*23*). Data acquired from image sets in counts/pixel were calibrated using the standard quantification procedures to report uptake values in Bq/cc.

Subjects were positioned on the scanner bed, and a whole body (top of the head to toes) CT scan was acquired for attenuation correction and localization of organs. Subsequently, 505 ± 96 MBq (13.6 ± 2.6 mCi) of ^{11}C-nicotine was injected intravenously into the subject's arm, and sequential PET scans were acquired in a 3-D mode over 90 min to provide a total of 14 scans (time-points). Prior to the first whole body PET scan, dynamic brain scans were acquired for the first 90 s commencing from the time of C-11 injection (45 frames, 2 s each), to capture the uptake and distribution characteristics of ^{11}C-nicotine in the brain. Subsequently, 12 whole body image sets (head to mid-thigh) were obtained using the following image acquisition sequence: 2 × 15 s, 3 × 20 s, 2 × 30 s, 3 × 60 s, and 2 × 90 s. After the twelfth whole body scan, a final image set covering the entire body from the top of the head to the toes was acquired (60 s/bed position). The PET images were reconstructed using the fully 3-D maximum likelihood ordered subset expected maximization algorithm, with 28 subsets, 2 iterations, and a 6 mm post loop filter (*23*).

PET image analysis and calculation of residence time

Reconstructed coronal images were used for the identification and measurement of the radioactivity content in key organs. Using PMOD 3.0 software (PMOD Technologies, Zurich, Switzerland), regions of interest (ROIs) were drawn manually across all image planes, for each image set, to determine total radioactivity accumulated in an organ. All ROIs were carefully drawn to minimize organ boundary edge artifacts, and were viewed in coronal, sagittal, and axial directions to ensure that different ROIs did not overlap. The CT images were utilized for secondary confirmation of the anatomical accuracy of the PET ROIs. Lumbar spine ROIs were used to calculate radioactivity in the red marrow. International Commission on Radiological Protection-89 guidelines were followed to estimate the quantity of red marrow in an adult, and were used to calculate the total amount of radioactivity accumulated in the bone marrow. Whole body muscle uptake was

calculated by multiplying the quantity of radioactivity present in a thigh muscle ROI by a weighting factor, as described in following equation.

$$\%ID_{Muscle} = \%ID_{Thigh\ Muscle\ ROI} * \frac{Weight\ *\ \%muscle\ mass}{Vol_{Thigh\ Muscle\ ROI} * \rho_{muscle}}$$

Additionally, a large 'whole body' ROI was created to calculate the quantity of radioactivity in the whole body. Time activity curves (TACs) were generated from each ROI, and the accumulated radioactivity in each organ was expressed as a percentage of the injected dose (%ID). For the residence time calculations, the radioactivity content beyond the last imaged time-point was assumed to be depleted exclusively by the physical decay of the radioactivity. Integration of the TAC data from time zero to complete elimination of radioactivity (area under the curve) was performed using the trapezoidal method to derive residence times for various organs.

Calculation of equivalent organ dose and effective dose

The absorbed radiation dose for individual organs was estimated by entering organ residence times into OLINDA/EXM 1.0 software (*24*). OLINDA utilizes the Medical Internal Radiation Dose scheme, and the dose estimates were obtained for the 70 kg adult male. Effective dose equivalent and radiation absorbed dose were determined using the methods published in the earlier International Commission on Radiological Protection publication 30 and 60, respectively (*25,26*).

RESULTS

The ^{11}C-nicotine was eluted from a semi-preparatory high performance liquid chromatography column in ~6.5–8.5 min with a radiochemical yield of ~30% and a radiochemical purity of >99%. The product was reconstituted in saline for injection, and sterile filtered using a 0.2 μ Millipore filter. The average specific activity (n = 16) of ^{11}C-nicotine was 264 ± 23 GBq/mmol (7158 ± 648 Ci/mmol) at the end of synthesis.

Following intravenous injection, the radioactivity accumulated in the brain rapidly. Representative brain PET images from one male and one female subject are shown in Fig. 1. The TACs generated from the brain images acquired during the first 90 sec for a representative male and a female subject is shown in Fig. 2. In general, a lag of ~8–10 s between the time of injection and arrival of radioactivity in the brain was noted. Comparing the radioactivity levels from the brain TACs of the representative male and female subjects, higher levels of radioactivity were noted in the female brains (Fig. 2). Besides the accumulation levels, these TACs also show a distinct difference in the rate of radioactivity accumulation between the male and female brains. The uptake slope during the initial phase (5-37 s) of radioactivity accumulation in the female and male brain was 1.06 (linear fit r^2=0.999) and 0.58 (linear fit r^2=0.997), respectively ($p < 0.001$). This initial rapid rise in radioactivity was followed by a much slower accumulation phase. The average slope during this slow uptake period was 0.22 (r^2=0.921) and 0.16 (r^2=0.941) in the female and male brains, respectively.

The whole body PET images show a rapid uptake and distribution of ^{11}C-nicotine for most major organs. Dividing the whole body ROI value with the decay corrected injected dose provided a recovery coefficient of 95% ± 7%. The PET image of a representative male and a female subject showing a typical whole body distribution pattern for ^{11}C-nicotine is shown in Fig. 3. The 2.8 min PET/CT images clearly delineated most major organs such as the brain, lungs, spleen, liver, and

kidneys (Fig. 3, top row). Because of urinary excretion was the primary route for radioactivity elimination, the urinary bladder was more distinct on the later images (Fig. 3, bottom row). The uptake in the right and left lung of a representative male and a female subject is shown in Fig. 4A and Fig. 4B, respectively. Average uptake in the left and right lung for all subjects is presented in Fig. 4C. The TACs generated for several of the major organs that were easily discernible on PET images are presented in Fig. 5. As seen from Fig. 5, after an initial rapid uptake, a significant washout of radioactivity was noted for most organs with time. For example, the %IDs of C-11 in the liver, brain, red marrow, muscle, and lungs was 9.4 ± 1.9, 6.2 ± 1.5, 5.0 ± 2.0, 15.2 ± 9.1, and 6.0 ± 2.2, respectively, at 2.8 min, and these levels decreased to 0.6 ± 0.2, 0.1 ±0.0, 0.3 ± 0.1, 1.2 ± 0.4, and 0.2 ± 0.0 by 86.5 min.

The residence time for each organ was computed by integrating the total accumulated radioactivity in the individual organ, from the time of injection to the complete elimination of the radioactivity. The mean residence times for various organs are shown in Table 1. The radiation absorbed dose for various organs was estimated by entering the residence times into the OLINDA software and is presented in Table 2. The four organs that received the highest radiation absorbed dose in this study were the urinary bladder wall (14.68 ± 8.70 μSv/MBq), kidneys (9.56 ± 2.46 μSv/MBq), spleen (9.49 ± 3.89 μSv/MBq), and liver (8.94 ± 1.67 μSv/MBq). The mean effective radiation dose to a 70 kg human was 5.44 ± 0.67 μSv/MBq (20.11 ± 2.47 mrem/mCi). The effective dose calculated in this study for the ^{11}C-nicotine is similar to values reported for many of the commonly used ^{11}C-labeled radiopharmaceuticals and comparison of the effective doses between ^{11}C-nicotine and certain commonly used ^{11}C-labeled radiopharmaceuticals are presented in Table 3.

DISCUSSION

Several investigators identified the advantages of using ^{11}C-nicotine PET to study nicotine addiction and neurodegenerative disease. A PET imaging study showed lower accumulation of ^{11}C-nicotine in the brains of Alzheimer's disease patients than in age matched healthy controls, implying the loss of nicotinic receptors in Alzheimer's disease (*27*). PET studies on patients with Alzheimer's disease were also effective in finding a direct correlation between ^{11}C-nicotine levels in the parietal cortex and the results of a clock drawing test (*16*). Another ^{11}C-nicotine PET imaging study investigated the influence of mentholated cigarettes on nicotine accumulation in the brain (*19*). These, and many other imaging studies conducted over the years, testify to the merits of ^{11}C-nicotine PET for a variety of applications (*19,20,28-32*). However, despite many ^{11}C-nicotine studies performed in humans, no dosimetry data have been presented. This study is the first to report on the radiation dosimetry of ^{11}C-nicotine derived from whole body PET/CT imaging performed in human subjects.

In this study, the PET images showed a rapid uptake of radioactivity in most organs leading to clear visualization of several organs with in few minutes of an intravenous injection of ^{11}C-nicotine (Fig. 3). Similarly, the radioactivity rapidly accumulated in the brain soon after the injection of ^{11}C-nicotine (Fig. 1). The TACs generated from the PET images revealed a lag of ~8–10 s between the time of injection and the arrival of radioactivity in the brain (Fig. 2). The radioactivity levels peaked in the brain within 90 s post-injection, with an initial sharp rise of radioactivity during the first 5–37 s, followed by a slow but sustained accumulation of radioactivity (Fig. 2). Regression analysis of this initial steep rise of radioactivity phase show a linear fit of data (r^2= 0.999 female; r^2=0.997 male), whereas the slower rise of accumulation show a non-linear fit (r^2=0.921 female; r^2=0.941 male). This pattern of steep rise of radioactivity followed by a slow but

sustained radioactivity accumulation pattern in the brain is similar to that reported previously by ourselves and others where the ^{11}C-nicotine was administered via the inhalation (*20,33*).

Although the TACs from the whole body PET images show a rapid but low uptake of ^{11}C-nicotine in major organs such as the heart, spleen, kidneys, liver, and lungs, most organs were easily delineated on the PET images (Fig. 3). The uptake intensity for the right side lung on PET images was slightly higher than that for the left lungs. The TACs from a representative male and a female subject and from the average of all subjects indicated slight higher but statistically insignificant levels of radioactivity accumulation in the right lungs (Fig. 4). Initial uptake in the lungs was followed by a rapid and significant washout of radioactivity. Similarly, several other major organs also showed a significant and steady washout of radioactivity with time. For example, the radioactivity in the liver and kidneys peaked within the first 5 min, and decreased ~15-fold by 86.5 min (Fig. 5). Similarly, the radioactivity in the blood pool was 26.1 ± 8.0 %ID at 2.78 min, and these levels decreased 45-fold to 0.6 ± 0.1%ID by 86.5 min. Although the muscles were not distinctly visible on the PET scans, the %ID in the muscles was significantly higher than in the liver and spleen (Fig. 5), the two tissues that were distinctly visible on the PET images. This anomaly could be due to the relatively higher muscle mass in the human body in comparison with the mass of liver and spleen. The bladder showed a steady rise of radioactivity with time for the duration of the scan due to the renal excretion of radioactivity from the body. Unlike the uptake pattern in the brain and the muscle, some other major organs show higher levels of ^{11}C-nicotine in the male subjects than seen for the female group (Fig 5). While notable, these uptake differences were statistically insignificant ($p > 0.1$).

The residence time for individual organs was calculated using the area under the curve from the TACs generated for those tissues from the PET images. The maximum residence time for ^{11}C-labeled radiopharmaceuticals is 0.488 h (*34*). The residence time for the remainder of the body

was obtained by subtracting the sum of the residence time for all of the identified tissues from 0.488 h. The residence times thus generated for various tissues agreed reasonably well across subjects, and were entered in the OLINDA software to derive the radiation absorbed dose for individual organs (Table 2). The estimated mean effective dose for ^{11}C-nicotine was 5.44 ± 0.67 μSv/MBq (20.11 ± 2.47 mrem/mCi) for a 70 kg human. The estimated effective dose equivalent for ^{11}C-nicotine was 5.71 ± 0.73 μSv/MBq (21.13 ± 2.70 mrem/mCi). The critical organs are the urinary bladder wall, kidneys, and spleen. Based on these calculated values, a standard injection of 555 MBq (15 mCi) of ^{11}C-nicotine would result in 3.02 mSv (0.3 rem) of exposure to a 70 kg human body. The current federal guidelines limit the radiation exposure for a research subject to a 0.03Sv (3 rem) effective dose for a single study, and 0.05 Sv (5 rem) effective dose for the whole year (*35*). This effective dose limit corresponds to administration of ~9250 MBq (~250 mCi) of ^{11}C-nicotine per subject/year. These results show that the radiation absorbed dose from ^{11}C-nicotine in human studies is relatively low. These results should help in planning future studies and in advising research subjects of potential risk associated with radiation dose from ^{11}C-nicotine PET studies.

CONCLUSION

In conclusion, we evaluated the whole body distribution and radiation dosimetry of ^{11}C-nicotine. The effective dose of ^{11}C-nicotine in a healthy subject is 5.4 μSv/MBq, thus suggesting only a modest radiation dose burden from a 555 MBq (15 mCi) injection of ^{11}C-nicotine. These results will be helpful in calculating the associated radiation dose burden when planning multiple PET studies with ^{11}C-nicotine on the same subject.

DISCLOSURE

The costs of publication of this article were defrayed in part by the payment of page charges. To solely indicate this fact, the article I hereby marked “advertisement” in accordance with 18 USC section 1734. No potential conflict of interest relevant to this article was reported.

ACKNOWLEDGEMENTS

We would like to acknowledge the skillful assistance of the staff at Wake Forest University Health Sciences Research PET center. Support from the Center for Biomolecular Imaging is also highly appreciated.

REFERENCES:

1. Jamal A, Homa DM, O'Connor E, et al. Current cigarette smoking among adults - United States, 2005-2014. *MMWR Morb Mortal Wkly Rep.* 2015;64:1233-1240.

2. Stolerman IP, Mirza NR, Shoaib M. Nicotine psychopharmacology: addiction, cognition and neuroadaptation. *Med Res Rev.* 1995;15:47-72.

3. Stolerman IP, Jarvis MJ. The scientific case that nicotine is addictive. *Psychopharmacology (Berl).* 1995;117:2-10; discussion 14-20.

4. Prevention CfDCa. Tobacco use among middle and high school students-United States, 2011-2015. *Morbity and Mortality Weekly Report.* 2016;65:361-367.

5. Doherty K, Kinnunen T, Militello FS, Garvey AJ. Urges to smoke during the first month of abstinence: relationship to relapse and predictors. *Psychopharmacology (Berl).* 1995;119:171-178.

6. George O, Ghozland S, Azar MR, et al. CRF-CRF1 system activation mediates withdrawal-induced increases in nicotine self-administration in nicotine-dependent rats. *Proc Natl Acad Sci U S A.* 2007;104:17198-17203.

7. Kenny PJ, Markou A. Conditioned nicotine withdrawal profoundly decreases the activity of brain reward systems. *J Neurosci.* 2005;25:6208-6212.

8. Goldberg SR, Spealman RD, Goldberg DM. Persistent behavior at high rates maintained by intravenous self-administration of nicotine. *Science.* 1981;214:573-575.

9. Harvey DM, Yasar S, Heishman SJ, Panlilio LV, Henningfield JE, Goldberg SR. Nicotine serves as an effective reinforcer of intravenous drug-taking behavior in human cigarette smokers. *Psychopharmacology (Berl).* 2004;175:134-142.

10. Watkins SS, Epping-Jordan MP, Koob GF, Markou A. Blockade of nicotine self-administration with nicotinic antagonists in rats. *Pharmacol Biochem Behav.* 1999;62:743-751.

11. Harrison AA, Gasparini F, Markou A. Nicotine potentiation of brain stimulation reward reversed by DH beta E and SCH 23390, but not by eticlopride, LY 314582 or MPEP in rats. *Psychopharmacology (Berl).* 2002;160:56-66.

12. Shiffman SM, Jarvik ME. Smoking withdrawal symptoms in two weeks of abstinence. *Psychopharmacology (Berl).* 1976;50:35-39.

13. Struble RG, Cork LC, Whitehouse PJ, Price DL. Cholinergic innervation in neuritic plaques. *Science.* 1982;216:413-415.

14. Warpman U, Nordberg A. Epibatidine and ABT 418 reveal selective losses of alpha 4 beta 2 nicotinic receptors in Alzheimer brains. *Neuroreport.* 1995;6:2419-2423.

15. Perry E, Martin-Ruiz C, Lee M, et al. Nicotinic receptor subtypes in human brain ageing, Alzheimer and Lewy body diseases. *Eur J Pharmacol.* 2000;393:215-222.

16. Kadir A, Almkvist O, Wall A, Langstrom B, Nordberg A. PET imaging of cortical (11)C-nicotine binding correlates with the cognitive function of attention in Alzheimer's disease. *Psychopharmacology (Berl).* 2006;188:509-520.

17. Nordberg A. PET studies and cholinergic therapy in Alzheimer's disease. *Rev Neurol (Paris).* 1999;155(Suppl 4):S53-S63.

18. Nordberg A. Nicotinic receptor abnormalities of Alzheimer's disease: therapeutic implications. *Biol Psychiatry.* 2001;49:200-210.

19. Zuo Y, Mukhin AG, Garg S, et al. Sex-specific effects of cigarette mentholation on brain nicotine accumulation and smoking behavior. *Neuropsychopharmacology.* 2015;40:884-892.

20. Rose JE, Mukhin AG, Lokitz SJ, et al. Kinetics of brain nicotine accumulation in dependent and nondependent smokers assessed with PET and cigarettes containing 11C-nicotine. *Proc Natl Acad Sci U S A.* 2010;107:5190-5195.

21. Halldin C, Nagren K, Swahn CG, Langstrom B, Nyback H. (S)- and (R)-[11C]nicotine and the metabolite (R/S)-[11C]cotinine. Preparation, metabolite studies and in vivo distribution in the human brain using PET. *Int J Rad Appl Instrum B.* 1992;19:871-880.

22. Teras M, Tolvanen T, Johansson JJ, Williams JJ, Knuuti J. Performance of the new generation of whole-body PET/CT scanners: Discovery STE and Discovery VCT. *Eur J Nucl Med Mol Imaging.* 2007;34:1683-1692.

23. Iatrou M RS, Manjeshwar RM, and Stearns CW. A fully 3D iterative image reconstruction algorithm incorporating data correction *IEEE 2004.* Vol 4; 2004:2493-2497.

24. Stabin MG, Sparks RB, Crowe E. OLINDA/EXM: the second-generation personal computer software for internal dose assessment in nuclear medicine. *J Nucl Med.* 2005;46:1023-1027.

25. ICRP-30. Limit for intakes of radionuclides by workers *Ann ICRP.* 1981;6:1-124.

26. ICRP-60. 1990 Recommendations of the international commission on radiological protection. *Ann ICRP.* 1991;21:1-201.

27. Nordberg A, Hartvig P, Lilja A, et al. Decreased uptake and binding of 11C-nicotine in brain of Alzheimer patients as visualized by positron emission tomography. *J Neural Transm Park Dis Dement Sect.* 1990;2:215-224.

28. Nyback H, Halldin C, Ahlin A, Curvall M, Eriksson L. PET studies of the uptake of (*S*)- and (*R*)-[^{11}C]nicotine in the human brain: difficulties in visualizing specific receptor binding in vivo. *Psychopharmacologia.* 1994;115:31-36.

29. Sharma A, Brody AL. In vivo brain imaging of human exposure to nicotine and tobacco. *Handb Exp Pharmacol.* 2009:145-171.

30. Lundqvist H, Langstrom B, Nordberg A. Use of carbon-11 nicotine in PET studies. *Eur J Nucl Med.* 1997;24:825-826.

31. Lernermarmarosh N, Carroll FI, Abood LG. Antagonism of nicotine's action by cocaine analogs. *Life Sci.* 1994;56:PL67-PL70.

32. Muzic RF, Jr., Berridge MS, Friedland RP, Zhu N, Nelson AD. PET quantification of specific binding of carbon-11 nicotine in human brain. *J Nucl Med.* 1998;39:2048-2054.

33. Berridge MS, Apana SM, Nagano KK, Berridge CE, Leisure GP, Boswell MV. Smoking produces rapid rise of [11C]nicotine in human brain. *Psychopharmacology (Berl).* 2010;209:383-394.

34. Hirvonen J, Roivainen A, Virta J, Helin S, Nagren K, Rinne JO. Human biodistribution and radiation dosimetry of 11C-(R)-PK11195, the prototypic PET ligand to image inflammation. *Eur J Nucl Med Mol Imaging.* 2010;37:606-612.

35. ICRP-1996. Radiological Protection and safety in medicine. *Ann ICRP.* 1996;73:26.

36. Scheinin NM, Tolvanen TK, Wilson IA, Arponen EM, Nagren KA, Rinne JO. Biodistribution and radiation dosimetry of the amyloid imaging agent 11C-PIB in humans. *J Nucl Med.* 2007;48:128-133.

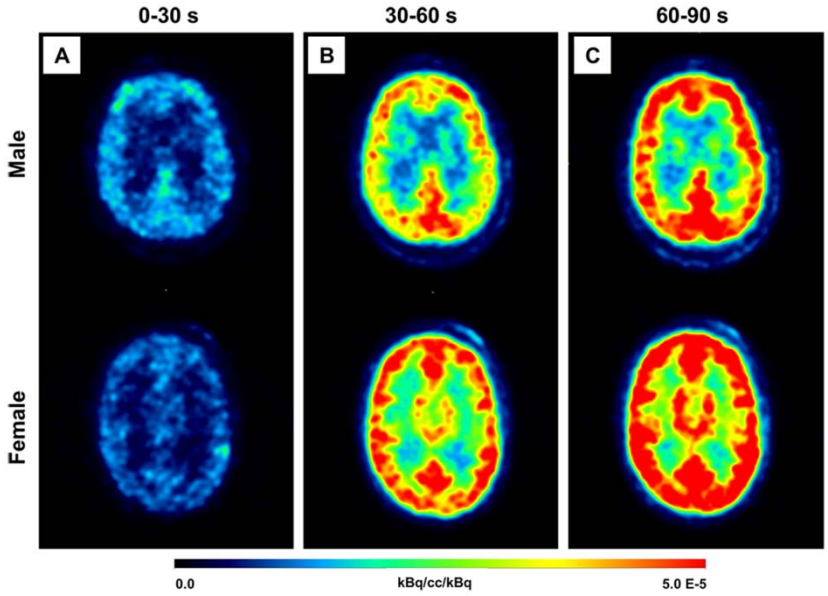

FIGURE 1. Axial view of representative brain PET images from one male (top row) and one female (bottom row) subject. PET scans were acquired dynamically over 90 sec (45 frames of 2 s each) after injection of ^{11}C-nicotine. The data for the two sets of images is normalized to injected dose. These 45 frames were divided into three image sets/groups *i.e.* 0-30 s (A), 0-60 sec (B), and 0-90 s (C). A higher accumulation was seen in the female brain as compared to the male brain (B and C).

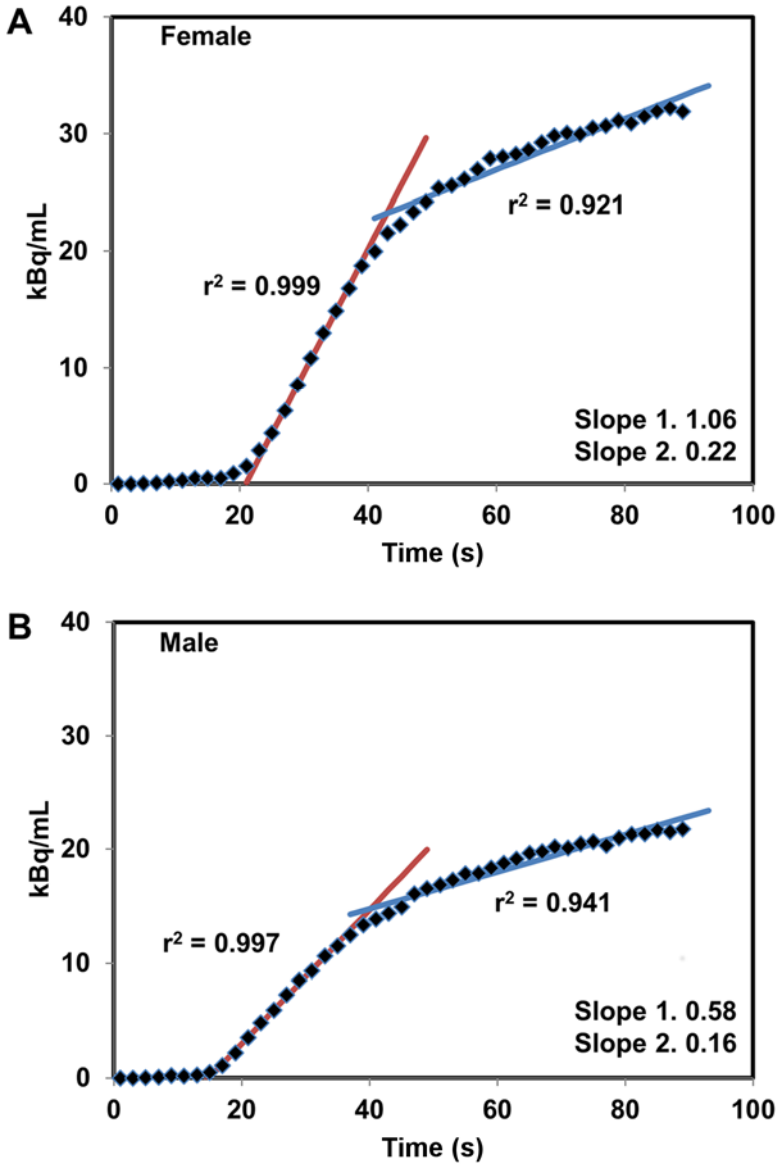

FIGURE 2. The time activity curves generated from the dynamic brain PET scans acquired over the first 90 s of a representative female (A) and a male subject (B). After an initial lag of ~ 10 sec between the injection and arrival or radioactivity in the brain, rapidly increasing levels were noted in the brain for both the groups. These TACs show an initial faster radioactivity accumulation phase (red line) followed by a much slower but sustained accumulation time period (Blue line).

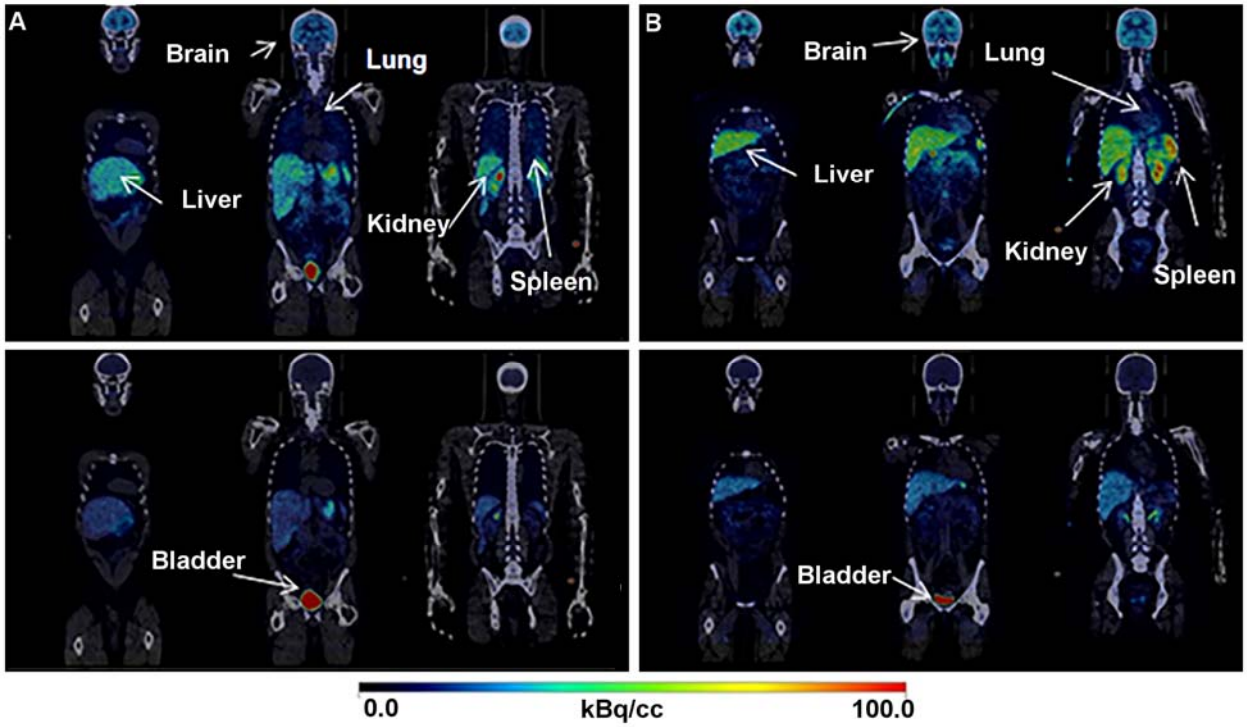

FIGURE 3. Coronal view of representative 2.8 min (top rows) and 22.6 min (bottom rows) whole body PET/CT images of a male (A) and a female (B) subject. The early images clearly delineate the brain, liver, spleen, lungs, and kidneys. The late images show an intense accumulation in the urinary bladder. The brain, liver, lungs, spleen, and kidneys are less conspicuous in the late images (bottom row) than seen in the early images (top row) indicating a significant washout/clearance of radioactivity from these organs with time.

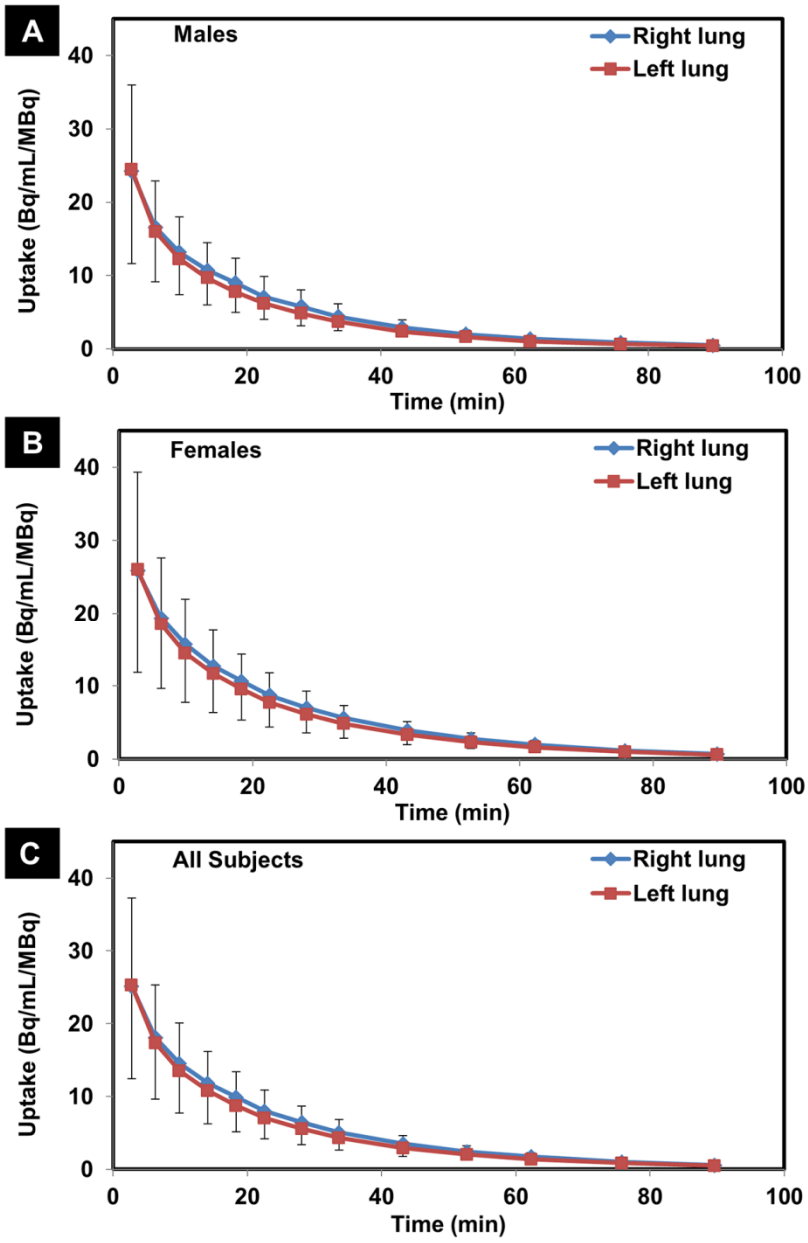

Figure 4: The time activity curve showing the accumulation of C-11 nicotine in the right and left lungs from a representative male (A) and female (B) subject. The average uptake in the right and left lungs from all subjects (an average of uptake) is shown in Fig. C. In all cases, slightly higher uptake was seen in the right lungs but these differences were statistically insignificant ($p>0.12$).

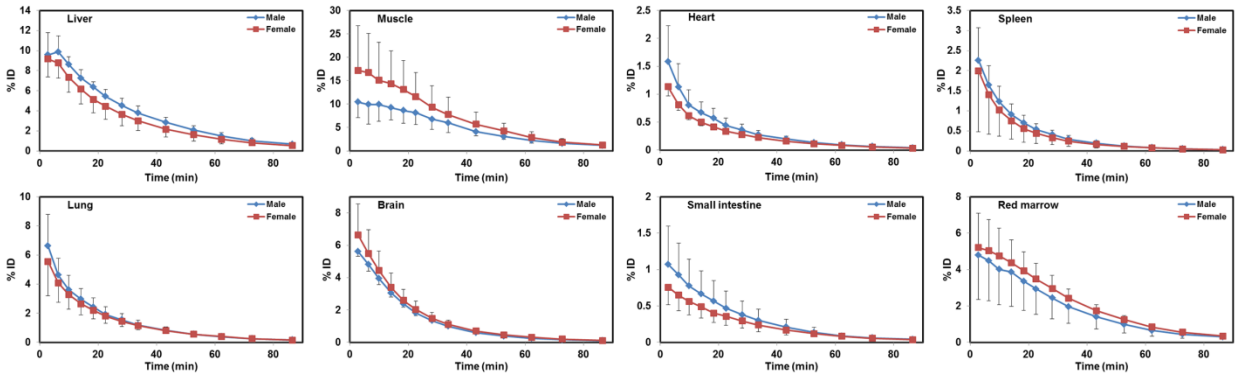

FIGURE 5. The time activity curves generated from the ROIs placed on organs that were easily discernible on the whole body PET/CT images. The radioactivity level in each organ is presented as the averaged percent of injected dose (%ID) for the male and the female groups. In general, the accumulation levels in most organs peaked during the first few minutes and then started to decrease rapidly with time.

TABLE 1

Residence times calculated from whole body images of 11 subjects injected with ^{11}C-nicotine

Organ	**Residence Time (h)**
Brain	0.021 ± 0.004
Liver	0.048 ± 0.010
Lung	0.020 ± 0.005
Bladder	0.019 ± 0.013
Kidney	0.009 ± 0.003
Muscle	0.088 ± 0.040
Red marrow	0.031 ± 0.005
Spleen	0.005 ± 0.003
Stomach	0.007 ± 0.004
Pancreas	0.001 ± 0.000
Heart	0.004 ± 0.001
Lower large intestine	0.005 ± 0.002
Small intestine	0.004 ± 0.002
Remainder of body	**0.227 ± 0.039**

TABLE 2

Radiation dose estimates for ^{11}C-nicotine (Mean ± SD)*

Organ	*Dose (µSv/MBq)*	*Dose mRem/mCi*
Adrenals	2.93 ± 0.20	10.85 ± 0.72
Brain	5.33 ± 0.98	19.74 ± 3.80
Breasts	1.75 ± 0.19	6.49 ± 0.70
Gallbladder wall	3.21 ± 0.26	11.86 ± 0.96
Lower large intestine wall	6.96 ± 1.75	25.75 ± 6.47
Small intestine	3.69 ± 0.54	13.65 ± 2.01
Stomach wall	6.00 ± 1.97	22.22 ± 7.28
Upper large intestine wall	2.63 ± 0.16	9.72 ± 0.59
Heart wall	3.65 ± 0.46	13.51 ± 1.70
Kidneys	9.56 ± 2.46	35.35 ± 9.08
Liver	8.94 ± 1.67	33.03 ± 6.14
Lungs	6.22 ± 1.24	23.03 ± 4.60
Muscle	2.01 ± 0.34	7.45 ± 1.24
Ovaries	2.72 ± 0.12	10.07 ± 0.45
Pancreas	4.29 ± 0.57	15.89 ± 2.13
Red marrow	5.15 ± 0.50	19.09 ± 1.83
Osteogenic cells	4.63 ± 0.33	17.15 ± 1.21
Skin	1.53 ± 0.12	5.65 ± 0.46
Spleen	9.49 ± 3.89	35.09 ± 14.36
Testes	1.91 ± 0.11	7.06 ± 0.42
Thymus	2.07 ± 0.16	7.67 ± 0.60
Thyroid	7.14 ± 1.00	26.41 ± 3.70
Urinary bladder wall	14.68 ± 8.70	54.35 ± 32.28
Uterus	2.92 ± 0.30	10.78 ± 1.11
Total body	2.81 ± 0.04	10.40 ± 0.15
Effective Dose Equivalent	**5.71 ± 0.73**	**20.11 ± 2.47**
Effective Dose	**5.44 ± 0.67**	**21.13 ± 2.70**

*(Mean ± Standard Deviation)

TABLE 3

Comparison of effective dose estimates between ^{11}C-nicotine and other ^{11}C-radiopharmaceuticals

	^{11}C-Nicotine#	**^{11}C-PIBδ**	**^{11}C-PK11195ε**
Urinary bladder wall	14.7	16.6	9.8
Kidneys	9.6	12.6	14.0
Spleen	9.5	4.3	12.5
Liver	8.9	19.0	9.5
Thyroid	7.1	2.4	1.9
Effective Dose	**5.4**	**4.7**	**4.8**

#: Current Study; Δ: Ref (*36*); Ɛ Ref(*34*)